

Accretion Disks Around Binary Black Holes: A Simple GR-Hybrid Evolution Model

Stuart L. Shapiro^{1,*}

¹*Department of Physics, University of Illinois at Urbana-Champaign, Urbana, IL 61801*

We consider a geometrically thin, Keplerian disk in the orbital plane of a binary black hole (BHBH) consisting of a spinning primary and low-mass secondary (mass ratio $q \lesssim 1$). To account for the principle effects of general relativity (GR), we propose a modification of the standard Newtonian evolution equation for the (orbit-averaged) time-varying disk surface density. In our modified equation the viscous torque in the disk is treated in full GR, while the tidal torque is handled in the Newtonian limit. Our GR-hybrid treatment is reasonable because the tidal torque is concentrated near the orbital radius of the secondary and is most important prior to binary-disk decoupling, when the orbital separation is large and resides in the weak-field regime. The tidal torque on the disk diminishes during late merger and vanishes altogether following merger. By contrast, the viscous torque drives the flow into the strong-field region and onto the primary during all epochs. Following binary coalescence, the viscous torque alone governs the time-dependent accretion onto the remnant, as well as the temporal behavior, strength and spectrum of the aftermath electromagnetic radiation from the disk. We solve our GR-hybrid equation for a representative BHBH-disk system, identify several observable EM signatures of the merger, and compare results obtained for the gas and EM radiation with those found with the Newtonian prescription.

PACS numbers: 98.62.Mw, 98.62.Qz

I. INTRODUCTION

Binary black hole (BHBH) mergers are likely to occur in regions immersed in gas, and the capture and accretion of the gas by the binary may result in appreciable electromagnetic radiation. There exists the realistic possibility of detecting electromagnetic “precursor” radiation prior to the merger and before the maximum gravitational wave (GW) emission from a BHBH merger [1, 2]. Then, following the detection of gravitational waves, observing electromagnetic “afterglow” radiation could provide further confirmation of the coalescence [3–9]. Such electromagnetic radiation can also serve as a useful probe of the gas in galaxy cores or in other regions where mergers take place, as well as a diagnostic of the physics of black hole accretion. This diagnostic may be particularly revealing once the masses and spins of the merging companions and BH remnant are determined from the GW signal.

In this paper we focus on a geometrically thin, Keplerian disk orbiting in the plane of a spinning BH with a low-mass companion. To follow the orbit-averaged, secular evolution of such a BHBH-disk system, a simplified, vertically integrated, $1 + 1$ - dimensional Newtonian model equation [Eq. (1) below] has been adopted in many previous studies (see, e.g., [1, 2, 10] and references therein). We have demonstrated how the steady-state solution to this equation can be used to determine the disk structure and electromagnetic radiation spectrum during the long inspiral epoch prior to binary-disk decoupling, during which a quasistationary treatment is applicable [11]. To illustrate this approach we solved the

steady-state equation for representative BHBH-disk systems at decoupling, employing simplified prescriptions for the required viscosity $\nu(r)$ and disk scale-height $h(r)$ profiles. Our steady-state approach was extended in [12], where the Shakura-Sunyaev [13] “one-zone” prescription for radiation transport was adopted in conjunction with a “ β ”-disk viscosity law to obtain these profiles self-consistently (see also [14]).

Here we provide an alternative evolution equation that better approximates the strong-field, relativistic nature of the circumbinary disk. This equation treats the viscous torque in full GR for gas flow in a thin Keplerian disk. The disk, which is not self-gravitating for densities of interest here, evolves in the background spacetime determined by the more massive primary, assumed to be a (quasi-)stationary Kerr black hole. The tidal torque, arising from the presence of the low-mass secondary, is handled in the Newtonian limit. The later approximation is reasonable since the tidal torque is strongly peaked in and just outside a narrow gap in the disk centered on the orbit of the secondary. This torque plays its most important role prior to binary-disk decoupling, when the binary separation is large and lies outside the strong-field region of the primary. Moreover, the tidal torque disappears altogether following merger. By contrast, the viscous torque drives gas into the strong-field region during all epochs, including the post-merger phase. A GR treatment of the viscous-driven accretion onto the primary and the post-merger remnant is particularly important for making predictions of any observable, ‘precursor’ and ‘aftermath’ electromagnetic radiation that may accompany the GW burst.

A fully reliable description of the accretion flow and associated radiation really requires a radiation magnetohydrodynamics (MHD) simulation in full general relativity in the $3 + 1$ -dimensional, dynamical spacetime of the

* Also Department of Astronomy and NCSA, University of Illinois at Urbana-Champaign, Urbana, IL 61801

merging BHBH binary. Newtonian hydrodynamic simulations incorporating some of the relevant physics have been performed in various dimensions and levels of approximation (see, e.g., [4, 6, 7, 15–17], while GR simulations are in their preliminary stages (e.g., [18–26]). Only recently have the first relativistic MHD simulations of a BHBH-disk system been performed: Noble et al. [27] adopt post-Newtonian gravitation to perform simulations of an equal-mass system, excising the region inside the binary orbit, while Farris et al. [28] summarize simulations in full GR that cover the complete spatial domain, including the black holes. Both of these relativistic MHD simulations deal primarily with geometrically thick (i.e. warm) disks in which an “effective viscosity” is provided by magnetic fields driven turbulent by the magnetorotational instability (MRI).

The model discussed here is mainly relevant for geometrically thin (i.e. cool) circumbinary disks. Although based on a simplified orbit-average description, it should delineate many of the qualitative features characterizing the evolution of BHBH-thin disk systems. Also, the model may be useful for selecting input parameters and identifying scaling behavior for future, more detailed numerical simulations. In addition, the resulting solutions can provide approximate initial disk profiles for such simulations. It is in this spirit and toward these purposes that we propose the adoption of our simple GR-hybrid equation. We hope that it provides a starting point for improved GR modeling along these lines.

In Section II we review the Newtonian binary-disk model and the required elements that enter the secular evolution equation. We also summarize how the resulting accretion rate onto the primary and the local electromagnetic flux and total luminosity from the disk can be calculated. Simplifications that arise when describing the pre-decoupling and post-merger epochs are summarized. In Section III we present the GR-hybrid model and retrace our previous discussion, now adapting it to the GR-hybrid equation. In Section IV we provide a numerical example by solving the equations for an illustrative BHBH-disk system. We begin our integrations prior to binary-disk decoupling and proceed through inspiral and merger, comparing the Newtonian and GR-hybrid solutions. In Section V we outline future work that will improve the model. We adopt geometrized units and set $G = 1 = c$ throughout.

II. THE NEWTONIAN EVOLUTION EQUATIONS

A. Disk Evolution

For reference and comparison we write down the standard Newtonian evolution equation for the surface den-

sity, $\Sigma(t, r)$,

$$\frac{\partial \Sigma}{\partial t} = -\frac{1}{2\pi r} \frac{\partial}{\partial r} \left[\left(\frac{\partial(r^2 \Omega)}{\partial r} \right)^{-1} \frac{\partial G}{\partial r} \right]. \quad (1)$$

Here $G \equiv -T_{\text{vis}} + T_{\text{tid}}$ is the total torque, T_{vis} is the viscous torque, T_{tid} is the tidal torque on the disk from the presence of the secondary, and $\Omega = \Omega_K = (M/r^3)^{1/2}$ is the Keplerian orbital frequency about the primary, centered at $r = 0$. The mass of the primary is M and the secondary qM , where $q \ll 1$. The viscous torque density is given by the standard equation [1, 2, 29, 30]

$$\frac{\partial T_{\text{vis}}}{\partial r} = -\frac{\partial}{\partial r} \left(2\pi r^3 \nu \Sigma \frac{\partial \Omega}{\partial r} \right). \quad (2)$$

We approximate the (orbit-averaged) tidal torque density by using the expression adopted by Armitage and Natarajan [1]

$$\frac{\partial T_{\text{tid}}}{\partial r} = 2\pi \Lambda \Sigma r \quad (3)$$

where $\Lambda(r, a)$ is given by

$$\Lambda = \begin{cases} - (fq^2 M/2r) (r/\Delta_p)^4, & r < a \\ + (fq^2 M/2r) (a/\Delta_p)^4, & r > a \end{cases}. \quad (4)$$

In Eq. (4) f is a dimensionless normalization factor and Δ_p is given by $\Delta_p = \max(|r-a|, h)$, and $a(t)$ is the orbital radius of the secondary. Calibrating the above expression for the tidal field against high-resolution, hydrodynamical simulations in two-dimensions for a low-mass, black hole secondary interacting with an outer accretion disk, Armitage and Natarajan find that the value $f \approx 0.01$ best fits the simulation results. Equations (3) and (4) furnish a reasonable analytic approximation to the results obtained from summing over the pointlike contributions from the Lindblad resonances in the disk [31, 32]. (Similar, but slightly different, forms for the tidal torque also have been used in the literature; see, e.g., [2, 33–35].

Assembling the above expressions then yields the final evolution equation

$$\frac{\partial \Sigma}{\partial t} = \frac{1}{r} \frac{\partial}{\partial r} \left[3r^{1/2} \frac{\partial}{\partial r} \left(r^{1/2} \nu \Sigma \right) - \frac{2\Lambda \Sigma r^{3/2}}{M^{1/2}} \right]. \quad (5)$$

The accretion rate through any radius r in the disk may be calculated from

$$\begin{aligned} \dot{M}(t, r) &= 2\pi r \Sigma(-v_r) \\ &= - \left[\frac{\partial(r^2 \Omega)}{\partial r} \right]^{-1} \frac{\partial G}{\partial r}. \end{aligned} \quad (6)$$

Combining Eqs. (1) and (6) yields

$$\frac{\partial \Sigma}{\partial t} = \frac{1}{2\pi r} \frac{\partial}{\partial r} \dot{M}. \quad (7)$$

To solve the above evolution equation we impose the following boundary conditions:

$$\text{b.c.'s : } \nu\Sigma = \begin{cases} (\nu\Sigma)_{\text{out}}, & r = r_{\text{out}} \\ 0, & r = r_{\text{isco}} \end{cases}. \quad (8)$$

In Eq. (8) r_{out} is the outer radius of the disk and r_{isco} is the ISCO radius of the primary. Typically, $r_{\text{out}} \gg r_{\text{isco}}$ and in some cases one can take $r_{\text{out}} \rightarrow \infty$. We retain the solution for finite r_{out} in part to facilitate numerical implementation of the outer boundary condition.

B. Orbital Evolution

The rate at which the secondary black hole migrates inward is determined both by back-reaction to the tidal torquing of the disk and by gravitational wave emission [2, 10]:

$$da/dt = (da/dt)_{\text{tid}} + (da/dt)_{\text{GW}}, \quad (9)$$

where

$$(da/dt)_{\text{tid}} = -\frac{4\pi a^{1/2}}{M^{3/2}q} \int_{r_{\text{isco}}}^{r_{\text{out}}} r \Lambda \Sigma dr \quad \left(\equiv \frac{a}{t_{\text{tid}}} \right), \quad (10)$$

and where $(da/dt)_{\text{GW}}$ is given by the familiar quadrupole-radiation orbital decay law,

$$(da/dt)_{\text{GW}} = -\frac{16 M^3 \zeta}{5 a^3} \quad \left(\equiv \frac{a}{t_{\text{GW}}} \right), \quad (11)$$

where $\zeta \equiv 4q/(1+q)^2$. In Eq. (10) the integration is over the entire disk, although most of the contribution from tidal torques arises close to the gap boundaries near $r \approx a$.

During any epoch in which back-reaction to tidal torques is not important, Eq. (9) can be integrated to yield

$$a(t)/a(0) = (1 - 4t/t_{\text{GW}}(0))^{1/4}, \quad t_{\text{GW}}/t_{\text{tid}} \ll 1, \quad (12)$$

where $t = 0$ marks the beginning of such an epoch.

C. Electromagnetic Radiation

The local radiated emission from the disk arises both from viscous and tidal dissipation. We assume that all of the dissipation is radiated locally, whereby the local electromagnetic flux $F(t, r)$ from each side of the disk is equal to the local dissipation rate $D(t, r)$ per unit surface area. The rate of viscous dissipation is [29]

$$D_{\text{vis}}(t, r) = \frac{9}{8} \nu \Sigma \frac{M}{r^3} = F_{\text{vis}}(t, r). \quad (13)$$

The rate of tidal dissipation is given by [10, 36]

$$D_{\text{tid}}(t, r) = \frac{1}{2} (\Omega(a) - \Omega(r)) \Lambda \Sigma = F_{\text{tid}}(t, r). \quad (14)$$

The local flux generates the luminosity $L(t, r)$ according to

$$\begin{aligned} \hat{F}_{\text{vis}}(t, r) &\equiv M^2 F_{\text{vis}}(t, r) / \dot{M}_{\text{eq}} \\ &= \frac{1}{4\pi} \left(\frac{M}{r} \right)^2 \frac{d}{d \ln r} \left(L_{\text{vis}}(t, r) / \dot{M}_{\text{eq}} \right), \end{aligned} \quad (15)$$

with a similar relation between $\hat{F}_{\text{tid}}(t, r)$ and $L_{\text{tid}}(t, r)$. The total local flux is then given by

$$\hat{F}(t, r) = \hat{F}_{\text{vis}}(t, r) + \hat{F}_{\text{tid}}(t, r), \quad (16)$$

and the total luminosity integrated over the entire disk (both sides) is

$$L(t) = L_{\text{vis}}(t) + L_{\text{tid}}(t). \quad (17)$$

In Eq. (15) \dot{M}_{eq} is the accretion rate in an *equilibrium* disk about a *single* black hole of mass M . When we compare Newtonian and GR-hybrid results we will use Eq. (33) for \dot{M}_{eq} in all of our normalizations.

D. Quasistationary Solution: Pre-Decoupling

As the binary inspiral proceeds from large separation, the inspiral timescale due to gravitational wave emission eventually becomes shorter than the viscous timescale in the disk, at which time the binary decouples from the disk and ultimately merges. We define the decoupling radius a_d to be the separation at which the two timescales become equal. Prior to BHBH-disk decoupling the balance between tidal and viscous torques drives the disk to a quasistationary equilibrium state, perturbed slightly by small amplitude, spiral density waves emanating from the edges of the gap. Previously we solved the disk evolution equations in steady state to determine the quasistationary, (orbit-averaged) surface density profile prior to decoupling as a function of the the binary separation [11]; see also [12, 14]. For these early epochs we set $a = \text{constant}$ and $\partial \Sigma / \partial t = 0$ in Eq. (5) to obtain the density profile. This quasistationary solution is used below as initial data for the Newtonian time-dependent simulations that evolve the binary-disk system from pre- to post-decoupling, continuing all the way through the late inspiral, merger and post-merger phases.

The accretion rate \dot{M} in steady state is independent of r . In steady state Eq. (5) admits a first integral which, when combined with Eq. (6), yields a first-order ODE,

$$\dot{M} = 2\pi \left[3r^{1/2} \frac{d(r^{1/2} \nu \Sigma)}{dr} - \frac{2\Lambda \Sigma r^{3/2}}{M^{1/2}} \right] = \text{constant}. \quad (18)$$

We could solve the second-order elliptic equation obtained by setting the right-hand side of Eq. (5) to zero to obtain the steady-state density profile, then evaluate Eq. (18) for the accretion rate. Alternatively, we could integrate the first-order Eq. (18) directly for the density,

which, when the boundary conditions are implemented, automatically provides \dot{M} as an eigenvalue. We chose the later strategy in [11], but adopt the former approach in Section IV B 1 in obtaining the initial data.

E. Quasistationary Solution: Post-Merger

Following binary merger the tidal torque vanishes while gas in the disk continues to diffuse inward on a viscous timescale, accreting onto the remnant black hole and ultimately settling into a final, stationary equilibrium state. This stationary disk configuration is described by well-known analytic density and temperature profiles, as well as analytic local fluxes and distant total luminosities, and these quantities provide useful checks on the late stages of any disk evolution calculation. The final equilibrium density profile, obtained by integrating Eq. (5) in steady-state in the absence of the tidal torque, is given by the familiar result for a Shakura-Sunyaev Newtonian thin disk around a single black hole (see, e.g., [30] and references therein), generalized for a disk of finite radial extent [11]:

$$\begin{aligned} \nu\Sigma(r) &= (\nu\Sigma)_{\text{out}} \frac{\left(1 - r_{\text{isco}}^{1/2}/r^{1/2}\right)}{\left(1 - r_{\text{isco}}^{1/2}/r_{\text{out}}^{1/2}\right)}, \quad [\text{post-merger}] \\ &= \frac{\dot{M}_{\text{eq}}}{3\pi} \left(1 - r_{\text{isco}}^{1/2}/r^{1/2}\right). \end{aligned} \quad (19)$$

The second equality above thus yields the steady-state accretion rate \dot{M}_{eq} in terms of the density and viscosity at the outer boundary:

$$\dot{M}_{\text{eq}} = 3\pi\nu_{\text{out}}\Sigma_{\text{out}} \frac{1}{1 - r_{\text{isco}}^{1/2}/r_{\text{out}}^{1/2}}. \quad (20)$$

The corresponding stationary flux, due entirely to viscous dissipation, may be expressed as

$$\hat{F}_{\text{vis}}(r) = \frac{3}{8\pi} \left(\frac{M}{r}\right)^3 \left(1 - r_{\text{isco}}^{1/2}/r^{1/2}\right). \quad (21)$$

The flux, together with Eq. (15), gives the differential luminosity,

$$\frac{d}{d \ln r} \left(L_{\text{vis}}(r)/\dot{M}_{\text{eq}}\right) = \frac{3}{2} \frac{M}{r} \left(1 - r_{\text{isco}}^{1/2}/r^{1/2}\right). \quad (22)$$

The total steady-state luminosity integrated over the entire disk is then given by

$$\begin{aligned} L_{\text{vis}} &= \frac{\dot{M}_{\text{eq}}M}{2r_{\text{isco}}} \left(1 - 3\frac{r_{\text{isco}}}{r_{\text{out}}} + 2\frac{r_{\text{isco}}^{3/2}}{r_{\text{out}}^{3/2}}\right), \quad [\text{post-merger}] \\ &= \frac{\dot{M}_{\text{eq}}M}{2r_{\text{isco}}}, \quad r_{\text{out}} \rightarrow \infty. \end{aligned} \quad (23)$$

III. THE GR-HYBRID EVOLUTION EQUATIONS

A. Disk Evolution

We propose the following GR-hybrid evolution equation for the rest-mass surface density ($\Sigma \equiv \int \rho_0 dz$, where ρ_0 is the rest-mass density) to replace Eq. (5):

$$\frac{\partial \Sigma}{\partial t} = \frac{1}{\Gamma r} \frac{\partial}{\partial r} \left[\frac{\Gamma}{Q} 3r^{1/2} \frac{\partial}{\partial r} \left(r^{1/2} \nu \Sigma \frac{\mathcal{D}^2}{\mathcal{C}} \right) - \frac{2\Lambda \Sigma r^{3/2}}{M^{1/2}} \right], \quad (24)$$

In assembling the above equation we specialized to the Kerr metric in Boyer-Lindquist coordinates to describe the (quasi-) stationary spacetime established by the more massive primary black hole. We used this metric to express the following functions, many of which were introduced by Novikov and Thorne [37] (see also Page and Thorne [38]):

$$\begin{aligned} M &= \text{mass of primary black hole,} \\ J &= \text{spin angular momentum of the primary hole,} \\ a_* &= J/M^2, \quad 0 \leq a_* \leq 1, \\ x &= (r/M)^{1/2}, \\ \Gamma &= \mathcal{B}\mathcal{C}^{-1/2}, \\ L^+ &= Mx\mathcal{C}^{-1/2}(1 - 2a_*x^{-3} + a_*^2x^{-4}), \\ Q &= 2x^{1/2}\partial L^+/\partial r, \\ \mathcal{B} &= 1 + a_*x^{-3}, \\ \mathcal{C} &= 1 - 3x^{-2} + 2a_*x^{-3}, \\ \mathcal{D} &= 1 - 2x^{-2} + a_*^2x^{-4}, \\ \mathcal{E} &= 1 - 2x^{-2} + a_*x^{-3}, \\ \mathcal{L} &= \text{Eq. (35) in [38],} \\ \mathcal{R} &= \mathcal{L}/\mathcal{B}. \end{aligned} \quad (25)$$

We note that in the case of a thin disk around a stationary Kerr black hole Σ as defined above is a scalar invariant, like ρ_0 .

Our proposed disk evolution Eq. (24) has the following features:

1. We assume that during all epochs the gas flow takes place in the background geometry of the more massive primary, which we approximate by the stationary Kerr metric. The viscous torque, described by the first term on the right-hand side, is treated in full GR for gas flow in a thin Keplerian disk. In the absence of the tidal torque term arising from the presence of the secondary, the equation reduces identically to the evolution equation presented in Lightman and Eardley [39] for time-dependent disk accretion onto a single Kerr black hole.
2. The tidal torque density, accounted for by the second term on the right-hand side, is based on the Newtonian formula, Eq.(3).
3. The entire equation reduces identically to Eq. (5) in the weak-field region, i.e., for $r/M \gg 1$, whereby $\Gamma, \mathcal{D}, \mathcal{C}$ and Q all approach unity.

4. In the absence of tidal torques, the steady-state solution of Eq. (24) gives the same profile for the product $\nu\Sigma$ that characterizes a standard relativistic Novikov-Thorne accretion disk around a single Kerr black hole [again generalized for a disk of finite radial extent; see Eq. (32)].

Basing the tidal torque on the Newtonian expression is motivated by the fact that this torque is strongly peaked near the orbit of the secondary and plays its most important role when the binary separation a is large. Specifically, the disk radii in which the torque is most significant typically satisfy $r \sim a \gg M$ and thus reside in the weak-field region outside the primary. (We neglect any accretion onto the secondary, which is expected to be small). By contrast, the viscous torque drives gas into the strong-field region and into the primary during all epochs and this flow requires a full GR treatment. Moreover, following merger, the tidal term vanishes and Eq. (24) reliably accounts for the inward diffusion of gas, the filling of any pre-merger gaps in the disk, the time-varying accretion onto the remnant, and the relaxation of the disk and accretion rate to a (quasi-)stationary state, all in full GR.

A more rigorous treatment would incorporate a relativistic tidal torque density dT_{tid}/dr in place of the Newtonian expression used here. Such a relativistic formula presumably can be obtained by employing the relativistic tidal torque derived by Hirata [40, 41] for a single Lindblad resonance in an accretion disk that orbits a Kerr black hole and is perturbed by a small secondary. This formula may be summed over many resonances, treated as a continuum, to get a smooth torque density. Such a sum has been carried out only for a Newtonian disk [31], and has been used here. However, as described above, employing this Newtonian formula in a first approximation should be adequate to treat many of the epochs of interest during the merger event.

To solve Eq. (24) we impose the same boundary conditions as specified by Eq. (8). The radius r_{isco} is given by the familiar expressions for a Kerr black hole in Boyer-Lindquist coordinates (see, e.g. [42], Eq. 12.7.24).

The *rest-mass* accretion rate through any radius r is given by

$$\begin{aligned} \dot{M}_0(t, r) &= 2\pi r \Sigma (-v^{\hat{r}}) \mathcal{D}^{1/2} \\ &= 2\pi \left[\frac{\Gamma}{Q} 3r^{1/2} \frac{\partial}{\partial r} \left(r^{1/2} \nu \Sigma \frac{\mathcal{D}^2}{\mathcal{C}} \right) - \frac{2\Lambda \Sigma r^{3/2}}{M^{1/2}} \right]. \end{aligned} \quad (26)$$

Combining Eqs. (24) and (26) then yields

$$\frac{\partial \Sigma}{\partial t} = \frac{1}{2\pi r \Gamma} \frac{\partial}{\partial r} \dot{M}_0. \quad (27)$$

Eqs. (26) and (27) reduce to Eqs. (6) and (7) in the Newtonian limit.

B. Orbital Evolution

The inspiral of a low-mass black hole companion onto a more massive primary is a nontrivial problem in general

relativity, even in vacuum. Post-Newtonian (PN) approaches, based on expansions in v^2/c^2 , can treat most of the inspiral epochs, but break down once the orbital separation shrinks to within a few times the radius of the massive primary. Treating the problem without approximation using the tools of numerical relativity is not computationally practical for following the inspiral from large separations characterizing binary-disk decoupling, but it can match onto PN trajectories at late times to continue the late-inspiral motion through plunge, merger and ring-down (for an overview and references, see [43]). However, numerical relativity cannot yet evolve binaries with mass ratios $q < 10^{-2}$ because of the excessive dynamic range and resulting resolution requirements. For such small mass ratios black hole perturbation theory provides the best approximation, although it is computationally and analytically expensive. One approach involves the calculation of the self-field acting on a test particle and following how it alters the orbital trajectory (For a status report and references see [44]). A simpler, but more approximate, method is the “radiative-adiabatic” scheme, where the inspiral is treated as a sequence of adiabatically shrinking geodesics. The shrinkage is determined by effectively calculating the rate of change of the constants of the motion (energy, angular momentum and Carter constant) due to GW emission. (For a summary and references see [45]). Simplifications arise for the case of interest here, where the orbit is nearly circular and resides in the equatorial plane of the primary.

It is therefore possible to modify Eq. (11) to obtain a more reliable expression for the orbital decay due to GW emission that accounts for higher-order general relativistic effects. Here, however, we will continue to use Eq. (11) for simplicity, as it is adequate to illustrate disk evolution via the GR-hybrid approach in a first approximation and can be generalized in subsequent analyses using the GR methods summarized above. Moreover, the deviations from the simple quadrupole approximation that arise when the secondary approaches the primary only lasts for a brief time interval, during which the bulk of the disk barely alters its structure. For the same reasons we will continue to use Eq. (10) to approximate the back-reaction of the tidal torque on the companion.

C. Electromagnetic Radiation

The local radiation flux $F_{\text{vis}}^{\text{com}}(t, r)$ removes the local viscous dissipation in the disk. Measured from each side of the disk per unit surface area by an observer comoving with the gas, it is given by

$$D_{\text{vis}} = F_{\text{vis}}^{\text{com}}(t, r) = \frac{3}{4} \left(\frac{M}{r^3} \right)^{1/2} \mathcal{W}(t, r) \frac{\mathcal{D}}{\mathcal{C}}, \quad (28)$$

where $\mathcal{W}(t, r)$ is the vertically-integrated shear stress [37],

$$\mathcal{W}(t, r) = \int dz t_{\hat{\phi}\hat{r}} = \frac{3}{2} \nu \Sigma \frac{M^{1/2}}{r^{3/2}} \frac{\mathcal{D}}{\mathcal{C}}. \quad (29)$$

We then define

$$\begin{aligned} \hat{F}_{\text{vis}}(t, r) &\equiv M^2 F_{\text{vis}}^{\text{com}}(t, r) / \dot{M}_{\text{eq}} \\ &= \frac{9}{8} \nu \Sigma \left(\frac{M}{r} \right)^3 \left(\frac{\mathcal{D}}{\mathcal{C}} \right)^2 / \dot{M}_{\text{eq}}, \end{aligned} \quad (30)$$

where \dot{M}_{eq} is the rest-mass accretion rate in an equilibrium disk about a single black hole of mass M (see Eq. 33). Consistent with our adopting Newtonian approximation for the tidal torque and tidal dissipation, we again use Eq. (14) for F_{tid} and define $\hat{F}_{\text{tid}}(t, r)$ by analogy with $\hat{F}_{\text{vis}}(t, r)$.

Following [46] we define a flux F in terms of the radiated energy as measured by a distant, stationary observer: $F(t, r) \equiv dE/(r dr d\phi dt) = -u_t F^{\text{com}}(t, r)$. Here E is the energy measured by the distant observer and u^α is the 4-velocity of a fluid element in a circular equatorial geodesic orbit about the primary: $u_t = -\tilde{\omega}^{\hat{0}} \cdot \partial/\partial t = -\mathcal{G}/\mathcal{C}^{1/2}$. Now the spacetime metric, which is dominated by the primary, is stationary. Moreover the orbit-averaged disk and its associated electromagnetic emission evolve on a slow, secular timescale ($\sim \min[t_{\text{vis}}, t_{\text{GW}}]$) during most phases. In this limit the total luminosity measured by a distant observer may be computed from $L(t) \equiv 2dE/dt = 4\pi \int F(t', r') r' dr'$ or $d(L/\dot{M}_{\text{eq}})/d(\ln r) = 4\pi r^2 F(t', r)/\dot{M}_{\text{eq}}$, where t' is the retarded time from the observer to the source (the ‘‘fast-light’’ approximation). We omit the small correction for any emitted radiation captured by the black holes.

D. Quasistationary Solution: Pre-Decoupling

The discussion in Section IID again applies. For binary separations $a \gg a_d$, the disk profile relaxes approximately to a quasistationary profile found by setting $\partial\Sigma/\partial t = 0$ in Eq. (24) and solving the resulting elliptic equation. We do so below in Section IV B 1 to determine the initial data for an evolution calculation. In this limit, the steady-state accretion rate \dot{M}_0 given by Eq. (26) satisfies

$$\dot{M}_0 = \text{constant}. \quad (31)$$

E. Quasistationary Solution: Post-Merger

Following black hole merger, a transient epoch ensues, wherein the gas diffuses inward toward the primary according to Eq. (24) in the absence of tidal torques and fills in any gaps that had been generated by the secondary. The disk eventually settles into a steady-state, relativistic Novikov-Thorne thin disk about the remnant black

hole, whereby the surface density satisfies $\partial\Sigma/\partial t = 0$, yielding

$$\begin{aligned} \nu\Sigma(r) &= (\nu\Sigma)_{\text{out}} \frac{\mathcal{C}^{3/2}}{\mathcal{C}_{\text{out}}^{3/2}} \frac{\mathcal{D}_{\text{out}}^2}{\mathcal{D}^2} \frac{\mathcal{R}}{\mathcal{R}_{\text{out}}}, \quad [\text{post-merger}] \\ &= \frac{\dot{M}_{\text{eq}}}{3\pi} \frac{\mathcal{C}^{3/2}}{\mathcal{D}^2} \mathcal{R}. \end{aligned} \quad (32)$$

Note that while Eq. (32) reduces to the Newtonian result, Eq. (19), as $r \rightarrow \infty$, the equilibrium profiles differ to $\mathcal{O}(M/r)^{1/2}$, a significant difference for gas near the remnant black hole. The second equality in Eq. (32) gives the steady-state, rest-mass accretion rate \dot{M}_{eq} in terms of the density and viscosity at the outer boundary:

$$\dot{M}_{\text{eq}} = 3\pi\nu_{\text{out}} \Sigma_{\text{out}} \frac{\mathcal{D}_{\text{out}}^2}{\mathcal{C}_{\text{out}}^{3/2} \mathcal{R}_{\text{out}}}. \quad (33)$$

The gas moves in a nearly circular geodesic orbit with an angular velocity

$$\Omega = \frac{M^{1/2}}{r^{3/2}} \frac{1}{\mathcal{B}}, \quad (34)$$

and an inward radial drift

$$v^{\hat{r}} = -\frac{3\nu}{2r} \left(\frac{\mathcal{D}}{\mathcal{C}} \right)^{3/2} \frac{1}{\mathcal{R}}, \quad (35)$$

as measured in the orthonormal orbiting frame. Combining Eqs. (30) and (32) yields the comoving stationary flux, which is now due entirely to viscous dissipation:

$$\hat{F}_{\text{vis}}(r) = \frac{3}{8\pi} \left(\frac{M}{r} \right)^3 \frac{\mathcal{R}}{\mathcal{C}^{1/2}}. \quad (36)$$

The flux results in a steady-state, differential luminosity,

$$\frac{d}{d \ln r} \left(L_{\text{vis}}(r) / \dot{M}_{\text{eq}} \right) = \frac{3}{2} \frac{M}{r} \frac{\mathcal{G}\mathcal{R}}{\mathcal{C}}. \quad (37)$$

Integrating Eq. (37) over the entire disk yields the total observed luminosity L_{vis} . For an infinite disk this integration yields

$$L_{\text{vis}} / \dot{M}_{\text{eq}} = 1 - \tilde{E}_{\text{iseco}} \quad (\equiv \eta), \quad r_{\text{out}} \rightarrow \infty, \quad (38)$$

where \tilde{E}_{iseco} is the binding energy per unit mass of a test particle in a circular geodesic orbit at r_{iseco} ,

$$\tilde{E}_{\text{iseco}} = \frac{r_{\text{iseco}}^2 - 2Mr_{\text{iseco}} + a_* M \sqrt{Mr_{\text{iseco}}}}{r_{\text{iseco}}(r_{\text{iseco}}^2 - 3Mr_{\text{iseco}} + 2a_* M \sqrt{Mr_{\text{iseco}}})^{1/2}}. \quad (39)$$

For a large, but finite disk with $M \ll r_{\text{out}} < \infty$ we have

$$\begin{aligned} L_{\text{vis}} / \dot{M}_{\text{eq}} &\approx 1 - \tilde{E}_{\text{iseco}} - 2 \int_{r_{\text{out}}}^{\infty} D_{\text{vis}} 2\pi r \, dr \\ &\approx 1 - \tilde{E}_{\text{iseco}} - \frac{3}{2} \frac{M}{r_{\text{out}}}. \end{aligned} \quad (40)$$

The right-hand side of Eq. (38) yields the well-known efficiency η of stationary accretion from an infinite disk onto a Kerr black hole: 5.72% for $a_* = 0$ and 42.3% for $a_* = 1$. The efficiency is less for a finite disk, as indicated by Eq. (40).

IV. NUMERICAL EVOLUTION

A. Nondimensionalization

To solve Eq.(24) numerically it is convenient to introduce the same nondimensional variables defined in [11]:

$$\begin{aligned} s &= (r/r_{\text{out}})^{1/2}, \quad s_1 = (a/r_{\text{out}})^{1/2}, \quad s_2 = (r_{\text{isco}}/r_{\text{out}})^{1/2}, \\ \bar{\Sigma} &= \Sigma/\Sigma_{\text{out}}, \quad \bar{\nu} = \nu/\nu_{\text{out}}, \quad y = s\bar{\Sigma}, \\ \bar{h} &= h/r, \quad \tau = t/2t_{\text{vis}}(r_{\text{out}}). \end{aligned} \quad (41)$$

Here

$$t_{\text{vis}}(r) = \frac{2}{3} \frac{r^2}{\nu} \quad (42)$$

is the characteristic viscous timescale at radius r in the disk.

In terms of these variables, equation (24) becomes

$$\frac{\partial y}{\partial \tau} = \frac{1}{\Gamma s^2} \frac{\partial}{\partial s} \left[\frac{\Gamma}{Q} \frac{\partial}{\partial s} \left(\bar{\nu} y \frac{\mathcal{D}^2}{\mathcal{L}} \right) - \frac{g^*(s)y}{(\max(|s^2 - s_1^2|, s^2 \bar{h}))^4} \right] \quad (43)$$

where

$$g^*(s) = \begin{cases} g s_1^8 & s > s_1 \\ -g s^8 & s < s_1 \end{cases}, \quad (44)$$

and where

$$g = \frac{2}{3} f q^2 \left(\frac{\nu_{\text{out}}}{M} \right)^{-1} \left(\frac{r_{\text{out}}}{M} \right)^{1/2} \quad (45)$$

Eq. (43) must be solved for $s \in [s_2, 1]$ subject to the boundary conditions

$$\text{b.c.'s:} \quad y = \begin{cases} 1, & s = 1 \\ 0, & s = s_2 \end{cases}. \quad (46)$$

We integrate Eq. (43) numerically, implementing a second-order, finite-difference, Crank-Nicholson scheme. Such an approach allows for arbitrarily large time-steps without the restriction of a Courant condition to insure stability. We choose a logarithmically increasing grid in radius to cover the large dynamic range in the disk with adequate spatial resolution everywhere.

B. A Numerical Example

To illustrate how a BHBH-disk system evolves when governed by the GR-hybrid equation we track a typical BHBH-disk system by integrating this equation in time. Following our approach in [11], we take the viscosity to have a power-law profile $\nu(r) \propto r^n$. We then specify the system by first choosing the parameters $q, a/M, r_{\text{out}}/M \gg 1$ and n . We determine the decoupling

separation a_d by the condition $t_{\text{GW}}(a_d) = \beta t_{\text{vis}}(2a_d)$ (setting $\beta = 0.1$), which yields

$$a_d/M = \left[\frac{128}{15 \cdot 2^n} \beta \zeta \left(\frac{\nu_{\text{out}}}{M} \right)^{-1} \left(\frac{r_{\text{out}}}{M} \right)^n \right]^{1/(n+2)}. \quad (47)$$

We next fix $\bar{h} = h/r = 0.1$, which essentially establishes the disk thickness near $r = a$, where it most matters. To set the scale for the density and disk size in physical units we fix Σ_{out} and r_{out} , which determine the disk mass M_{disk} . Finally, we set ν_{out} by specifying the final accretion rate onto the black hole remnant for an *infinite* disk, $\dot{M}_{\text{rem}} = 3\pi\nu_{\text{out}}\Sigma_{\text{out}}$ (see Eqs. 20 or 33 in the limit $r_{\text{out}} \gg M$) to be a fraction γ of the Eddington value, $\gamma = \dot{M}_{\text{rem}}/\dot{M}_{\text{Edd}}$. Here $\dot{M}_{\text{Edd}} \equiv L_{\text{Edd}}/\eta = 4\pi M m_p/(\eta\sigma_T)$, where m_p is the proton mass, σ_T is the Thomson cross-section and η is the radiative efficiency [see Eq. (38)]. This condition yields

$$\nu_{\text{out}}/M = \frac{4}{3} \frac{\gamma}{\eta} \frac{m_p}{\sigma_T \Sigma_{\text{out}}}. \quad (48)$$

As in [11], we assign the values $n = 0.5$ and $q = 5 \times 10^{-3}$ and set $f = 0.01$, $r_{\text{out}} = 10^3 M$, $\gamma = 0.1$, and $\Sigma_{\text{out}} = 1.5 \times 10^4 \text{g cm}^{-2}$. Our choice of parameters gives $M_{\text{disk}}/M_{\odot} \sim 5 \times 10^3 M_8^2$ ($M_8 \equiv M/10^8 M_{\odot}$), which is safely smaller than the mass of the secondary BH for all $M \lesssim 2 \times 10^{11} M_{\odot}$. These values for the asymptotic disk density and disk mass are comparable to cases considered in [1, 2]. We also set $J/M^2 = 0.5$, which gives $r_{\text{isco}} = 4.23M$. *The value of the primary mass M scales out of the problem* when solved in dimensionless form according to Eq. (43).

The adopted parameters give a decoupling radius $a_d/M = 18.1$ and a dimensionless tidal torque parameter $g = 0.0194$ [see [11], Eq. (35), for definition].

A more sophisticated treatment could adopt a one-zone approach as in a Shakura-Sunyaev or Novikov-Thorne disk. There one employs a local radiation prescription that yields the local temperature and pressure for an α -disk or β -disk viscosity law, and uses these to derive the viscosity and h/r profiles self-consistently (see, e.g. [12, 14]). However, the simplified, but physically plausible, assignments chosen here are sufficient for illustrating the implementation of the GR-hybrid equation (where we merely take it out for a “test-drive”) and we postpone a more detailed analysis for a future investigation.

1. Initial Data

We start the evolution when the binary separation is at $a/M = 5a_d/M = 90.3$. We thus begin to track the inspiral before binary-disk decoupling, when for much of the disk the evolution is still quasistationary. We can therefore set the initial density profile Σ to the quasistationary profile found by setting $\partial\Sigma/\partial t = 0$ in Eq. (24)

(i.e., $\partial y/\partial \tau = 0$ in Eq. 43) and solving the resulting elliptic equation, as discussed in Section III D.

At $t = 0$ we have $\tilde{g} = 9.68$, where the quantity \tilde{g} is defined by Eq. (55) of [11] and is related to g according to

$$\tilde{g} = \frac{1}{2}g \left(\frac{a}{r_{\text{out}}} \right)^{(1/2-n)} \left(\frac{h(a)}{a} \right)^{-3}. \quad (49)$$

As shown in that reference, \tilde{g} measures the ratio of the tidal to viscous torque on the disk at $r \sim a$. Whenever $\tilde{g} \gtrsim a$ a few prior to merger the dimensionless accretion rate satisfies $\dot{m} \ll 1$, i.e., the accretion rate onto the primary is much reduced below the value it would have in the absence of tidal torques from the secondary. At $t = 0$ we find $m = 1.03 \times 10^{-2}$, consistent with this expectation. Note that \tilde{g} decreases rapidly with increasing \bar{h} . Hence for thicker disks with $\bar{h} \gtrsim 0.1$, \tilde{g} would be smaller and there could be little or no suppression of accretion by the secondary (cf. [12]).

At $t = 0$ we find $t_{\text{GW}}/t_{\text{tid}} = 0.0588M_8$. This ratio, which measures the relative importance of tidal to gravitational radiation back-reaction forces on the secondary, decreases as the inspiral proceeds. Hence tidal back-reaction is not important in this particular scenario for all $M < 10^9$. Accordingly, we use Eq. (12) to track the orbital separation, consistent with the discussion in Section III B.

To assist in the interpretation of the numerical results and figures below, we list the following conversion of nondimensional to physical units applicable to this scenario:

$$\begin{aligned} t(\text{yrs}) &= 0.7649 \times 10^5 M_8 \tau, \\ a_d(\text{au}) &= 17.84 M_8, \\ \dot{M}_{\text{eq}}(M_\odot \text{ yr}^{-1}) &= \gamma \dot{M}_{\text{Edd}} \mathcal{P}_{\text{out}} = 0.3028 M_8, \\ L_{\text{eq}}(\text{erg s}^{-1}) &= \gamma L_{\text{Edd}} \mathcal{P}_{\text{out}} = 1.409 \times 10^{45} M_8. \end{aligned} \quad (50)$$

The subscript 'eq' refers to final quasistationary values associated with accretion onto the black hole remnant. The factor $\mathcal{P}_{\text{out}} \equiv \mathcal{P}_{\text{out}}^2 / (\mathcal{C}_{\text{out}}^{3/2} \mathcal{R}_{\text{out}})$ corrects for a relativistic disk which is *finite* and not infinite, as is the case here (cf. Eq. 33).

2. Evolution

The surface density profile is plotted at selected times during the evolution in Fig. 1. A gap forms in the disk near the orbital radius of the secondary at $r = a(t)$ and moves with the secondary as it spirals inward. Disk-binary decoupling occurs after $a(t)$ has reached a_d , which happens at $\tau = 0.05360$ ($t = 4.099 \times 10^3 M_8$ yrs). Prior to that time, the density profile evolves in a quasistationary manner and remains close to the quasistationary solution obtained by setting $\partial \Sigma / \partial t = 0$ at each orbital separation $a(t) > a_d$. Tidal torques, which are strongest near the orbital radius of the secondary, cause a pile-up of the

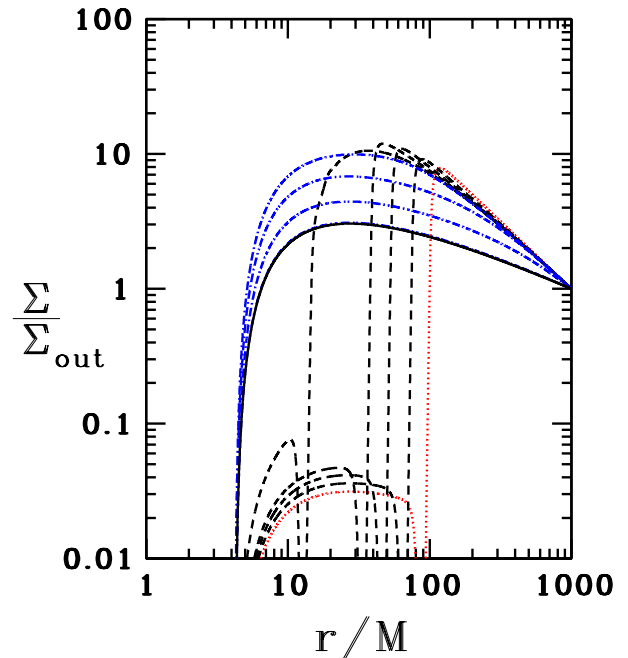


FIG. 1. Snapshots of the disk surface density profile at selected times. Profiles are shown for the initial disk at $\tau = 0$ (dotted red line), the final equilibrium disk at $\tau = \infty$ (solid black line) and for several intermediate times, $\tau = 0.03707, 0.04943, 0.05251, 0.05366$ (pre-merger dashed black lines) and $0.05406, 0.06178, 0.09267, 0.2471$ (post-merger dotted-dashed blue lines). Decoupling occurs at $\tau = 0.05360$ ($t = 4.099 \times 10^3 M_8$ yrs), and merger occurs at $\tau = 0.05368$ ($t = 4.106 \times 10^3 M_8$ yrs).

matter and create a density peak just outside $r = a(t)$. As the orbital radius shrinks, the peak surface density moves inward while steadily increasing. After merger, which occurs at $\tau = 0.05368$ ($t = 4.106 \times 10^3 M_8$ yrs or $\Delta t = 6.57 M_8$ yrs after decoupling), the tidal torques vanish altogether while the residual viscous torques drive the inward diffusion of gas toward the remnant black hole. This inward diffusion reduces the peak value of the density and eliminates the gap inside $r = a_d$ altogether. By $\tau = 0.2471$ ($\Delta t = 1.479 \times 10^4 M_8$ yrs after merger), the density profile is seen in the figure to be nearly indistinguishable from the equilibrium Novikov-Thorne solution for a relativistic disk accreting onto a single black hole, Eq. (32). The density at the ISCO vanishes at all times, as it is one of the boundary conditions.

The rest-mass accretion rate as a function of radius is plotted at select times in Fig. 2. At $t = \tau = 0$ the accretion rate, given by Eq. (26), is everywhere constant. Such a result is a consequence of demanding that $\partial \Sigma / \partial t = 0$ for the initial disk (see Eq. 27). The normalized value of the initial accretion rate, $\dot{M}/\dot{M}_{\text{eq}} = 1.031 \times 10^{-2}$, is much less than unity, the value characterizing an equilibrium disk with the same asymptotic density and viscosity about an isolated black hole. As discussed above and

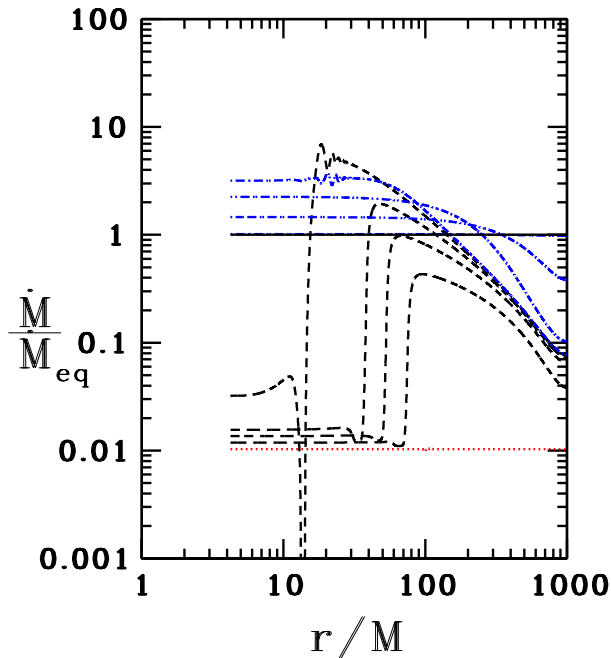


FIG. 2. Snapshots of the rest-mass accretion rate at selected times. Profiles are plotted at the same times shown in Fig. 1.

in [11], such a suppression of accretion flow is expected due to the high initial value of the torque parameter \tilde{g} . As the inspiral proceeds, the exact cancellation of the viscous and tidal torque terms in Eq. (26) breaks down and the mass flux grows behind the secondary. Soon after decoupling, the flow rate reaches values that actually *exceed* the final equilibrium value for an isolated black hole by almost a factor ~ 10 near $r \sim a_d$, as the tidal torques holding back the flow diminish in strength and the density pile-up abates (the “bursting of the dam”). Following merger the accretion rate eventually settles down to the constant equilibrium value, Eq. (33), throughout the disk.

It is interesting to compare the surface density profiles determined by integrating the GR-hybrid and Newtonian evolution equations for the same primary and secondary black hole masses, disk parameters (i.e. $\Sigma_{\text{out}}, \nu_{\text{out}}, r_{\text{ISCO}}, r_{\text{out}}, n, f$ and h/r) and secondary orbit $a(t)$. In each case the initial data is determined by setting $\partial\Sigma/\partial t = 0$ in their respective evolution equation and solving the resulting elliptic equation. The comparison is provided in Fig. 3. The initial quasistationary profiles are nearly identical, except in the strong-field region $r/M \lesssim 20$, where the Newtonian profile is higher. (A comparison of profiles in the strong-field region is of course influenced by gauge effects arising from the choice of radial coordinate, but Σ is a scalar invariant). The initial accretion rates are also slightly different (e.g. $\dot{M}/\dot{M}_{\text{eq}} = 0.8892 \times 10^{-2}$ in the Newtonian case), since the elliptic equations that determine the rates are different in the strong-field region. Prior to merger but after

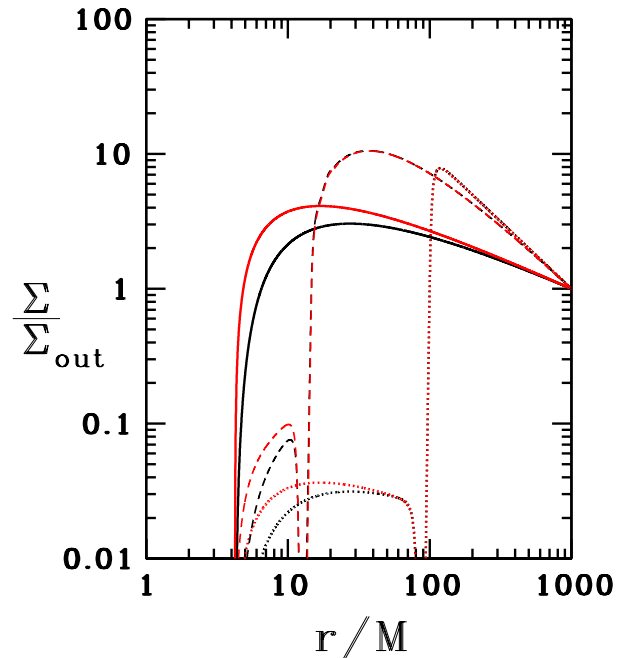


FIG. 3. Comparison of GR-hybrid and Newtonian disk surface density profiles at selected times. Profiles are shown for the initial disk at $\tau = 0$ (*dotted lines*), the final equilibrium disk at $\tau = \infty$ (*solid lines*) and at one intermediate time $\tau = 0.05366$ (pre-merger *dashed lines*). GR-hybrid lines are in *black* and Newtonian lines in *red*; for each line type the lower (upper) curves are the GR-hybrid (Newtonian) lines. Merger occurs at $\tau = 0.05368$ ($t = 4.106 \times 10^3 M_8$ yrs).

decoupling, the density profiles outside the orbital radius are close, but inside that radius they continue to depart. After merger, the equilibrium profiles in the strong field regime remain different: the peak value of the surface density is higher in the Newtonian case by 35%. The differences between the Newtonian and GR-hybrid solutions become more pronounced as the primary spin increases and $a_* \rightarrow 1$.

Profiles of the nondimensional comoving flux emerging from each side of the disk are plotted at selected times in Fig. 4. The evolution of the flux is correlated with the evolution of the disk surface density. The peak flux occurs just outside the orbital radius of the secondary prior to merger, and the regions where the flux dips correspond to the density gaps near that orbit. Prior to merger, the tidal torque-driven density pile-up causes the peak flux to increase with increasing time and decreasing orbital radius. Following merger the tidal torque vanishes and the flux begins to decrease everywhere. Eventually the flux, now generated by viscous dissipation alone, settles into the equilibrium state corresponding to steady accretion of gas in a thin, relativistic disk onto a single black hole [Eq. (36)] The flux vanishes at the ISCO.

A comparison of the comoving fluxes determined from the GR-hybrid and Newtonian evolution equations is presented in Fig. 5. Prior to merger the flux profiles are

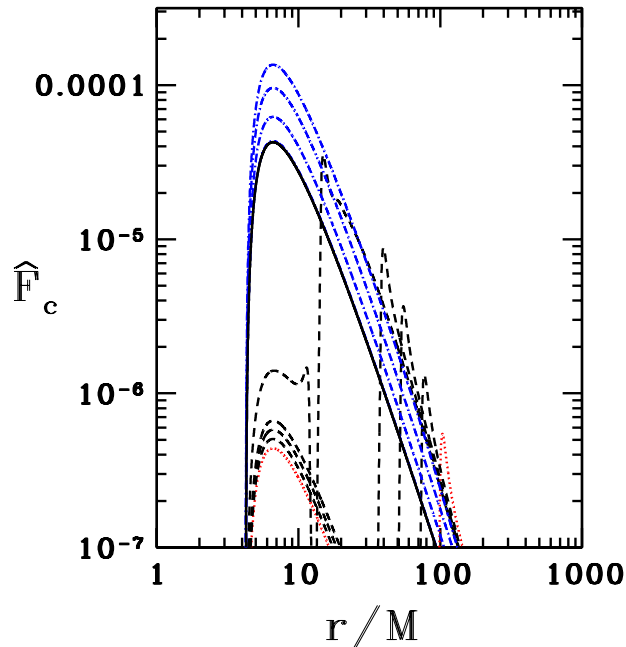


FIG. 4. Snapshots of the comoving flux profile at selected times. Profiles are plotted at the same times shown in Fig. 1.

quite comparable but after merger the final equilibrium profiles to which the disks relax differ significantly in the strong-field region $r/M \lesssim 15$. The peak value of the final equilibrium comoving flux is a factor of 2.1 times larger in the Newtonian case.

The ratio of the contribution of tidal heating to viscous heating to the comoving flux is plotted as a function of radius at selected times prior to merger in Fig. 6. Tidal heating dominates over viscous heating near $r = a(t)$, but decreases rapidly both at smaller and larger radii. [Note that exactly at $r = a(t)$ the tidal dissipation vanishes in accord with Eq. (14), hence the sudden dip in the curves]. This sudden fall-off is anticipated because the tidal torque, due to the presence of the secondary, decreases rapidly with distance from the secondary.

The contribution from various radii in the disk to the luminosity measured by a distant observer is plotted in Fig. 7 at selected times. The evolution of this quantity follows the general trends already found for the comoving flux shown in Fig. 4. The same differential luminosity function (up to our normalization) has been plotted in [46] for relativistic, Novikov-Thorne thin disks undergoing steady-state accretion onto single Kerr black holes, where they are compared with three-dimensional GRMHD simulations of thin disks ($h/r \lesssim 0.1$) that relax to steady-state; see their Fig. 1. Our post-merger luminosities are all driven to these Novikov-Thorne solutions at late times. The GRMHD results are in general agreement with these solutions, but do exhibit some emission inside the ISCO, plus a small inward shift of the peak emission to lower radii (see also [47]). These differences

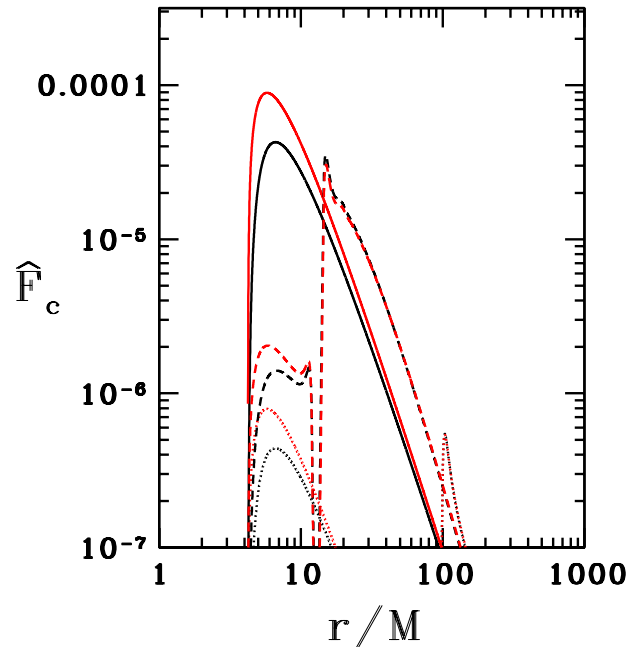


FIG. 5. Comparison of GR-hybrid and Newtonian disk comoving flux profiles at selected times. Profiles are plotted at the same times shown in Fig. 3.

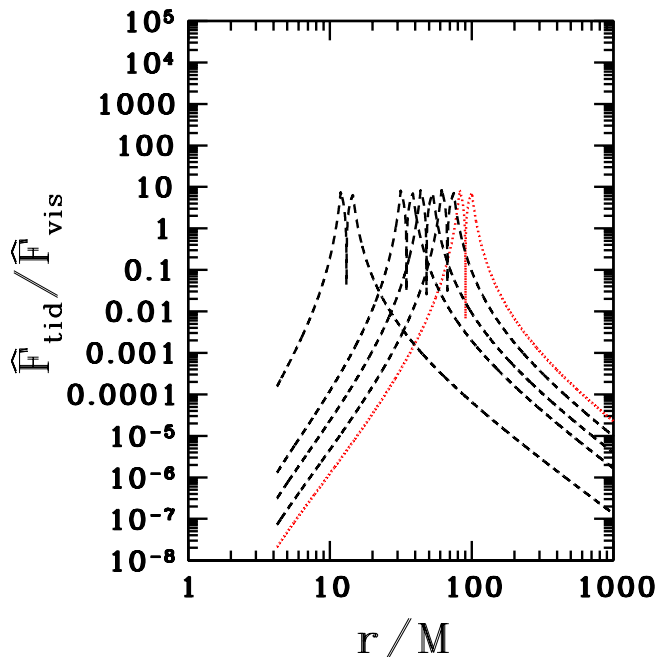


FIG. 6. Snapshots of tidal-to-viscous comoving flux profiles at selected times. Profiles are plotted at the same times shown in Fig. 1 *prior* to merger; following merger tidal dissipation vanishes.

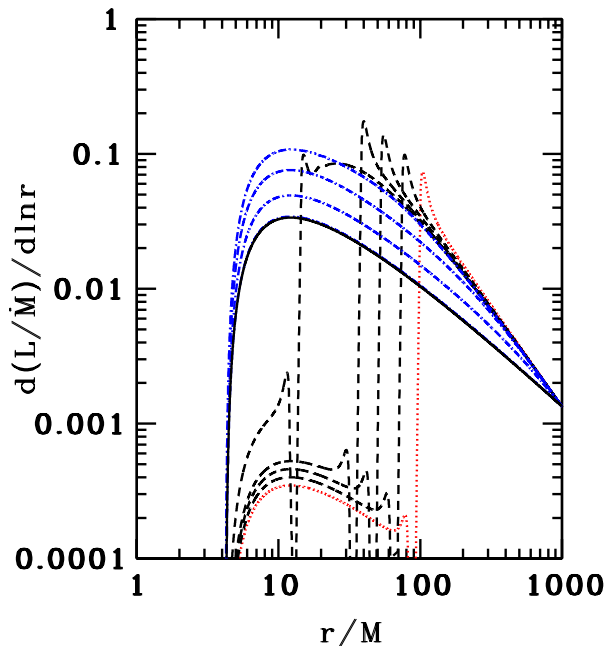


FIG. 7. Snapshots of the differential luminosity profile, which shows the contribution from various radii in the disk to the distant luminosity, is plotted at selected times. Profiles are plotted at the same times shown in Fig. 1.

are not deemed significant enough to affect the accuracy of, e.g., the continuum-fitting method, which employs the Novikov-Thorne model to estimate black hole spins.

The evolution of the total electromagnetic luminosity from the disk measured by a distant observer is plotted in Fig. 8. There it is seen that the tidal dissipation is always less important overall than viscous dissipation and vanishes altogether following merger. The luminosity rises sharply after merger, reaching a peak at $\tau = 0.0542$ and decaying slowly thereafter to its final, equilibrium value. The peak value is a full 3.08 times larger than its final equilibrium value given by Eq. 40, $L_{\text{eq}} = 0.0806\dot{M}_{\text{eq}}$. The rapid decline of the tidal torques following decoupling and the sudden inward drift of matter from $r \sim a_d$ is responsible for the overshoot in luminosity. The full width at half-maximum of the luminosity curve is $\Delta\tau = 0.03126$ ($\Delta t = 2.39 \times 10^3 M_8$ yrs). The rise, fall and asymptotic flattening of the luminosity curve may provide an electromagnetic signature that a BHBH merger has occurred in a circumbinary disk.

Also shown in Fig. 8 are the Newtonian evolution curves for the same quantities. The results are qualitatively similar, but the equilibrium accretion rates and radiation efficiencies are different from the GR-hybrid solution (e.g., $L_{\text{eq}} = 0.117\dot{M}_{\text{eq}}$, or 45% higher, in the Newtonian case) and the peak luminosity overshoot is somewhat smaller (about 15% lower in the Newtonian case).

Fig. 9 shows that the evolution of the total electromagnetic luminosity is correlated with the evolution of

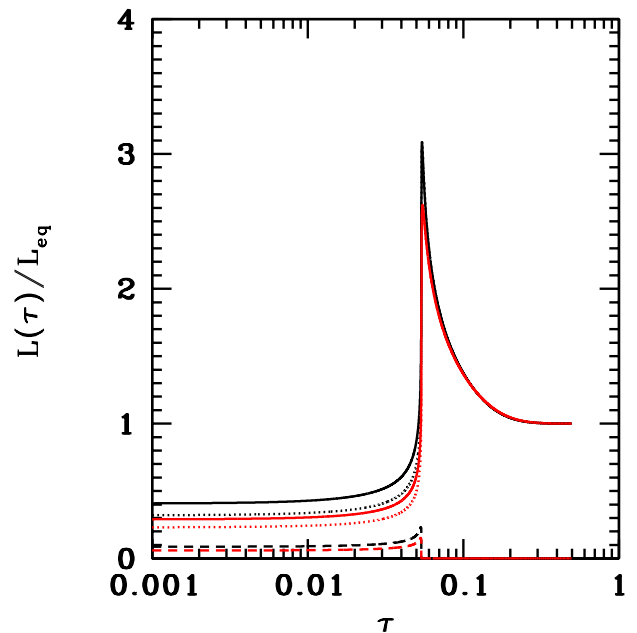


FIG. 8. Variation of the distant total disk luminosity with time. The *dashed* lines show the contribution from tidal dissipation, the *dotted* lines from viscous dissipation. The *solid* lines show the total luminosity. GR-hybrid lines are in *black* and Newtonian lines in *red*; for each line type the upper (lower) curves are the GR-hybrid (Newtonian) lines. Merger occurs at $\tau = 0.05368$ ($t = 4.106 \times 10^3 M_8$ yrs).

the accretion rate at the ISCO of the primary black hole. The overshoot of the accretion rate above the final equilibrium value, and its subsequent decay to the Novikov-Thorne value, drives the same time variation seen for the total luminosity.

As in the case of thin-disk accretion onto a single, stationary black hole, Newtonian and GR models for low-mass BHBH-disk systems typically give the same *qualitative* results for the observable EM radiation. Newtonian calculations are thus sufficient to identify characteristic EM luminosities and wavelengths. But the numerous factors of a \sim few that comprise the *quantitative* differences between the models are important if one hopes to use detailed observations to infer BH spins and other system parameters. For more complicated scenarios than the one analyzed here there can even be qualitative differences involving relativistic effects that must be taken into account (e.g., binary remnant recoil, misaligned BH spins, accretion jets, etc.).

V. FUTURE WORK

The numerical scenario summarized here is presented as a simple demonstration of the use of the GR-hybrid approach to track the orbit-averaged evolution of a thin,

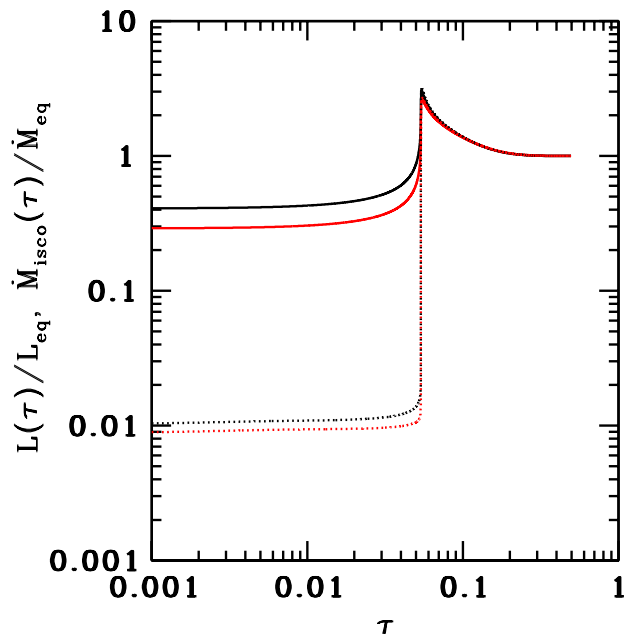


FIG. 9. Variation of the distant total disk luminosity (*solid lines*) and ISCO accretion rate (*dotted lines*) with time. GR-hybrid lines are in *black* and Newtonian lines in *red*; for each line type the upper (lower) curves are the GR-hybrid (Newtonian) lines. Merger occurs at $\tau = 0.05368$ ($t = 4.106 \times 10^3 M_8$ yrs).

Keplerian disk orbiting a low-mass BHBH, accounting for

some of the most important effects of general relativity. More detailed microphysics, combined with a parameter survey, will be necessary to fully explore the consequences of this model. Future applications should incorporate the following:

1. A self-consistent treatment of the viscosity and h/r profiles by implementing a Shakura-Sunyaev-Novikov-Thorne one-zone description of each ring in the disk, employing a local radiation prescription together with an α -disk or β -disk law for the viscosity to obtain the required profiles;

2. A calculation of the observed radiation spectrum, by employing a ray-tracing or Monte-Carlo technique, adapted to a time-dependent relativistic disk in curved spacetime (see, e.g. [48–50]).

Several GR refinements can be implemented to improve the model while retaining the spirit of an orbit-averaged description of an evolving BHBH-thin disk system. They include the following:

1. The replacement of the Newtonian formula with a fully relativistic expression for the tidal torque density, along the lines discussed in Section III A;

2. Employing the true relativistic inspiral trajectory for the low-mass BH companion, calculated using one of the GR techniques discussed in Section III B.

We intend to implement some of these improvements and apply the resulting formalism in future studies.

Acknowledgments: It is a pleasure to thank C. Gammie and V. Paschalidis for useful discussions and helpful comments. This paper was supported in part by NSF Grant PHY09-63136 and NASA Grants NNX11AE11G and NNX13AH44G to the University of Illinois at Urbana-Champaign.

-
- [1] P. J. Armitage and P. Natarajan, *ApJL* **567**, L9 (Mar. 2002)
 - [2] P. Chang, L. E. Strubbe, K. Menou, and E. Quataert, *Mon. Not. R. Astro. Soc.* **407**, 2007 (Sep. 2010)
 - [3] M. Milosavljević and E. S. Phinney, *ApJL* **622**, L93 (Apr. 2005)
 - [4] E. M. Rossi, G. Lodato, P. J. Armitage, J. E. Pringle, and A. R. King, *Mon. Not. R. Astro. Soc.* **401**, 2021 (Jan. 2010), arXiv:0910.0002 [astro-ph.HE]
 - [5] J. D. Schnittman and J. H. Krolik, *Astrophys. J.* **684**, 835 (Sep. 2008)
 - [6] L. R. Corrales, Z. Haiman, and A. MacFadyen, *Mon. Not. R. Astro. Soc.* **404**, 947 (May 2010), arXiv:0910.0014 [astro-ph.HE]
 - [7] S. M. O’Neill, M. C. Miller, T. Bogdanović, C. S. Reynolds, and J. D. Schnittman, *Astrophys. J.* **700**, 859 (Jul. 2009)
 - [8] S. L. Shapiro, *Phys. Rev. D* **81**, 024019 (Jan. 2010), 0912.2345 [astro-ph.HE]
 - [9] T. Tanaka and K. Menou, *Astrophys. J.* **714**, 404 (May 2010), arXiv:0912.2054 [astro-ph.CO]
 - [10] G. Lodato, S. Nayakshin, A. R. King, and J. E. Pringle, *Mon. Not. R. Astro. Soc.* **398**, 1392 (Sep. 2009), arXiv:0906.0737 [astro-ph.CO]
 - [11] Y. T. Liu and S. L. Shapiro, *Phys. Rev. D* **82**, 123011 (Dec. 2010), arXiv:1011.0002 [astro-ph.HE]
 - [12] B. Kocsis, Z. Haiman, and A. Loeb, *Mon. Not. R. Astro. Soc.* **427**, 2680 (Dec. 2012), arXiv:1205.5268 [astro-ph.HE]
 - [13] N. I. Shakura and R. A. Sunyaev, *A&A* **24**, 337 (1973)
 - [14] R. R. Rafikov, *ArXiv e-prints*(May 2012), arXiv:1205.5017 [astro-ph.GA]
 - [15] A. I. MacFadyen and M. Milosavljević, *Astrophys. J.* **672**, 83 (Jan. 2008)
 - [16] J.-M. Shi, J. H. Krolik, S. H. Lubow, and J. F. Hawley, *Astrophys. J.* **749**, 118 (Apr. 2012), arXiv:1110.4866 [astro-ph.HE]
 - [17] D. J. D’Orazio, Z. Haiman, and A. MacFadyen, *ArXiv e-prints*(Oct. 2012), arXiv:1210.0536 [astro-ph.GA]
 - [18] M. Megevand, M. Anderson, J. Frank, E. W. Hirschmann, L. Lehner, S. L. Liebling, P. M. Motl, and D. Neilsen, *Phys. Rev. D* **80**, 024012 (Jul. 2009), arXiv:0905.3390 [astro-ph.HE]
 - [19] M. Anderson, L. Lehner, M. Megevand, and D. Neilsen, *Phys. Rev. D* **81**, 044004 (Feb. 2010)
 - [20] B. D. Farris, Y. T. Liu, and S. L. Shapiro, *Phys. Rev. D*

- 81**, 084008 (Apr. 2010), arXiv:0912.2096 [astro-ph.HE]
- [21] T. Bode, R. Haas, T. Bogdanović, P. Laguna, and D. Shoemaker, *Astrophys. J.* **715**, 1117 (Jun. 2010)
- [22] P. Mösta, C. Palenzuela, L. Rezzolla, L. Lehner, S. Yoshida, and D. Pollney, *Phys. Rev. D* **81**, 064017 (Mar. 2010), arXiv:0912.2330 [gr-qc]
- [23] C. Palenzuela, T. Garrett, L. Lehner, and S. L. Liebling, *Phys. Rev. D* **82**, 044045 (Aug. 2010)
- [24] O. Zanotti, L. Rezzolla, L. Del Zanna, and C. Palenzuela, *A & A* **523**, A8 (Nov. 2010), arXiv:1002.4185 [astro-ph.HE]
- [25] B. D. Farris, Y. T. Liu, and S. L. Shapiro, *Phys. Rev. D* **84**, 024024 (Jul. 2011), arXiv:1105.2821 [astro-ph.HE]
- [26] T. Bode, T. Bogdanović, R. Haas, J. Healy, P. Laguna, and D. Shoemaker, *Astrophys. J.* **744**, 45 (Jan. 2012), arXiv:1101.4684 [gr-qc]
- [27] S. C. Noble, B. C. Mundim, H. Nakano, J. H. Krolik, M. Campanelli, Y. Zlochower, and N. Yunes, *Astrophys. J.* **755**, 51 (Aug. 2012), arXiv:1204.1073 [astro-ph.HE]
- [28] B. D. Farris, R. Gold, V. Paschalidis, Z. B. Etienne, and S. L. Shapiro, *Physical Review Letters* **109**, 221102 (Nov. 2012), arXiv:1207.3354 [astro-ph.HE]
- [29] J. E. Pringle, *Ann. Rev. Astron. Astrophys.* **19**, 137 (1981)
- [30] J. Frank, A. King, and D. J. Raine, *Accretion Power in Astrophysics* (Cambridge University Press, Cambridge, 2002)
- [31] P. Goldreich and S. Tremaine, *Astrophys. J.* **241**, 425 (Oct. 1980)
- [32] K. Hourigan and W. R. Ward, *Icarus* **60**, 29 (Oct. 1984)
- [33] D. N. C. Lin and J. Papaloizou, *Astrophys. J.* **309**, 846 (Oct. 1986)
- [34] W. R. Ward, *Icarus* **126**, 261 (Apr. 1997)
- [35] P. Chang, *Astrophys. J.* **684**, 236 (Sep. 2008), arXiv:0801.2133
- [36] J. Goodman and R. R. Rafikov, *Astrophys. J.* **552**, 793 (May 2001), arXiv:astro-ph/0010576
- [37] I. D. Novikov and K. S. Thorne, in *Black Holes, Les Houches*, edited by C. Dewitt and B. DeWitt (Gordon and Breach, New York, 1973) pp. 343–450
- [38] D. N. Page and K. S. Thorne, *Astrophys. J.* **191**, 499 (Jul. 1974)
- [39] D. M. Eardley and A. P. Lightman, *Astrophys. J.* **200**, 187 (Aug. 1975)
- [40] C. M. Hirata, *Mon. Not. R. Astro. Soc.* **414**, 3198 (Jul. 2011), arXiv:1010.0758 [astro-ph.HE]
- [41] C. M. Hirata, *Mon. Not. R. Astro. Soc.* **414**, 3212 (Jul. 2011), arXiv:1010.0759 [astro-ph.HE]
- [42] S. L. Shapiro and S. A. Teukolsky, *Black Holes, White Dwarfs, and Neutron Stars: The Physics of Compact Objects* (John Wiley, New York, 1983)
- [43] T. W. Baumgarte and S. L. Shapiro, *Numerical Relativity: Solving Einstein's Equations on the Computer* (Cambridge University Press, Cambridge, 2010)
- [44] E. Poisson, A. Pound, and I. Vega, *Living Reviews in Relativity* **14**, 7 (Sep. 2011), arXiv:1102.0529 [gr-qc]
- [45] N. Yunes, A. Buonanno, S. A. Hughes, Y. Pan, E. Barausse, M. C. Miller, and W. Thrope, *Phys. Rev. D* **83**, 044044 (Feb. 2011), arXiv:1009.6013 [gr-qc]
- [46] A. K. Kulkarni, R. F. Penna, R. V. Shcherbakov, J. F. Steiner, R. Narayan, A. Sä Dowski, Y. Zhu, J. E. McClintock, S. W. Davis, and J. C. McKinney, *Mon. Not. R. Astro. Soc.* **414**, 1183 (Jun. 2011), arXiv:1102.0010 [astro-ph.HE]
- [47] A. Sądowski, *Astrophys. J. Suppl.* **183**, 171 (Aug. 2009), arXiv:0906.0355 [astro-ph.HE]
- [48] J. C. Dolence, C. F. Gammie, M. Mościbrodzka, and P. K. Leung, *Astrophys. J. Suppl.* **184**, 387 (Oct. 2009), arXiv:0909.0708 [astro-ph.HE]
- [49] R. V. Shcherbakov and L. Huang, *Mon. Not. R. Astro. Soc.* **410**, 1052 (Jan. 2011), arXiv:1007.4831 [astro-ph.HE]
- [50] F. H. Vincent, T. Paumard, E.ourgoulhon, and G. Perrin, *Classical and Quantum Gravity* **28**, 225011 (Nov. 2011), arXiv:1109.4769 [gr-qc]